

RSC Advances



This is an *Accepted Manuscript*, which has been through the Royal Society of Chemistry peer review process and has been accepted for publication.

Accepted Manuscripts are published online shortly after acceptance, before technical editing, formatting and proof reading. Using this free service, authors can make their results available to the community, in citable form, before we publish the edited article. This *Accepted Manuscript* will be replaced by the edited, formatted and paginated article as soon as this is available.

You can find more information about *Accepted Manuscripts* in the [Information for Authors](#).

Please note that technical editing may introduce minor changes to the text and/or graphics, which may alter content. The journal's standard [Terms & Conditions](#) and the [Ethical guidelines](#) still apply. In no event shall the Royal Society of Chemistry be held responsible for any errors or omissions in this *Accepted Manuscript* or any consequences arising from the use of any information it contains.

Cite this: DOI: 10.1039/c0xx00000x

www.rsc.org/xxxxxx

ARTICLE TYPE

Hedgehog-like hierarchical ZnO needle-clusters with superior electron transfer kinetics for dye-sensitized solar cells

Jie Qu,^a Yongan Yang,^d Qingduan Wu,^c Paul R. Coxon,^b Yingjun Liu,^b Xiong He,^b Kai Xi,^{*b} Ningyi Yuan^a and Jianning Ding^{*a}

Received (in XXX, XXX) Xth XXXXXXXXX 20XX, Accepted Xth XXXXXXXXX 20XX
DOI: 10.1039/b000000x

Hedgehog-like hierarchical ZnO needle-clusters, three-dimensional (3-D) ZnO flowers and one-dimensional (1-D) ZnO needles have been synthesised via a facile hydrothermal method. These samples with different morphologies and microstructures were used to fabricate photoelectrodes for dye-sensitized solar cells (DSSCs). Out of the three samples, current-voltage (I-V) curve measurements show that DSSCs with hedgehog-like ZnO needle-clusters display the best photoelectrochemical performance which can be attributed to enhanced light harvesting and faster reaction kinetics resulting from the unique morphology. The UV-vis absorption and diffused reflectance spectra indicate that hedgehog-like ZnO needle-clusters show higher light harvesting abilities due to high UV absorption, stronger light scattering, as well as a high surface area. Electrochemical impedance spectroscopy (EIS), intensity-modulated photocurrent spectroscopy (IMPS), and intensity-modulated voltage spectroscopy (IMVS) further demonstrate that hedgehog-like ZnO needle-clusters provide superior electron transfer kinetics: fast electron transfer and long electron lifetimes with suppressed recombination. The ZnO needle-clusters obtained not only provide a 3-D matrix but also avoid extensive grain boundary formation. The discoveries from this work are important for the design of efficient photoanode materials with optimum structures for DSSCs.

1. Introduction

Dye-sensitized solar cells (DSSCs) have received considerable attention as a promising cost-effective alternative to conventional silicon semiconductor solar cells.¹⁻⁷ The efficiency-determining component of DSSCs is the semiconductor photoanode due to the competition between electron separation and recombination accompanying many electron transfer processes.⁸⁻¹⁰ This depends on the nature, morphology and structure of the nanocrystalline semiconductor oxide.¹¹⁻¹⁷ DSSCs with nanostructured TiO₂ electrodes have been investigated extensively.¹⁸⁻²² Until now the most successful DSSCs, with photoelectric conversion efficiencies of over 12%, have been reported using porous TiO₂ nanoparticle films,²³ which is based on extensive research focusing on TiO₂ photoanodes.²⁴⁻²⁸ Simultaneously, much of the current research focuses on using a series of other wide-band-gap semiconductor materials as potential alternatives to TiO₂.²⁹⁻³²

Among these metal oxides, ZnO has been considered a prime photoelectrode material candidate due to its similar electronic band (3.37 eV) structure to TiO₂, higher electron mobility (10² cm² V⁻¹ s⁻¹) and comparable electron injection efficiency.³³⁻³⁴ In addition, ZnO exhibits a diverse range of morphologies due to the ease of crystallization and controllable anisotropic growth compared with TiO₂.³⁵ These properties of ZnO could be generated in a wide variety of nano morphologies, consequently

constructing unique properties for DSSCs. Furthermore, previous reports have indicated the lifetime of electrons in ZnO electrodes is much longer than in those made from TiO₂, and the use of ZnO as the photoanode can effectively reduce the recombination rate of the electrons.³⁶ To date, much research has been devoted to the synthesis of ZnO nanomaterials with diverse morphologies and structures for use as photoanodes, such as zero-dimensional (0-D) nanoparticles,³⁷⁻⁴⁰ one-dimensional (1-D) nanostructures,⁴¹⁻⁴³ and three dimensional (3-D) nanoarchitectures.⁴⁴⁻⁴⁶

Morphology features of ZnO such as orientation and size, obviously have a crucial effect on the electron transfer processes in the semiconductor electrode. For conventional photoelectrode films made from ZnO particles³⁷⁻⁴⁰ the high surface area provided is adequate for dye loading, but the numerous grain boundaries existing between the nanocrystalline particles block the electron transport. 1-D ZnO nanostructures have a relatively small number of grain boundaries which reduces the grain boundary effect so the photoanode can provide a direct conduction pathway for rapid electron transport.⁴⁷⁻⁴⁹ However, it is difficult for the liquid electrolyte to penetrate into 1-D ZnO owing to the relatively low surface area with intact surface, which usually leads to a large interface charge-transfer resistance in 1-D nanostructured material-based electrode films. In addition, the low surface area of 1-D nanostructure reduces dye loading and light harvesting. Therefore, the energy conversion efficiencies of 1-D ZnO DSSCs usually remain at relatively low levels.

In this paper, a simple hydrothermal method is used to fabricate 1-D ZnO needles, 3-D ZnO flowers and 3-D hedgehog-like ZnO needle-clusters, respectively. Charge transfer kinetics of the different morphologies is investigated and contrasted. Compared with ZnO needles and ZnO flowers, hedgehog-like ZnO needle-clusters show the superior kinetical features: fast electron transfer and long electron lifetime. For DSSC applications such hedgehog-like structures show enhanced photoelectrochemical properties.

2. Experimental

2.1 Sample preparation and characterization

ZnO needles: an alkaline aqueous solution (1 M, 15 ml) was added to zinc nitrate solution (0.04 M, 25 ml) and stirred. After stirring for 2 h, the resulting solution was transferred to a Teflon-lined autoclave and heated to 100 °C for 5 h. The hot solid product was recovered and rinsed with distilled water.

ZnO flowers: alkaline aqueous solution (1 M, 15 ml) was added to zinc nitrate solution (0.04 M, 25 ml) with stirring. After stirring for 5 minutes, the resulting solution was transferred to a Teflon-lined autoclave immediately and then heated to 100 °C for 5 h. The hot solid product was recovered and rinsed with distilled water.

Hedgehog-like ZnO needle-clusters: alkaline aqueous solution (0.2 M, 15 ml) was added to zinc nitrate solution (0.04 M, 25 ml) with stirring for 5 minutes. The resulting solution was then transferred to a Teflon-lined autoclave immediately and heated to 100 °C for 5 h. The hot solid product was recovered and rinsed with distilled water.

Characterization: The structure and morphology of the final products was measured by X-ray diffraction (XRD, Rigaku D/max-2500) and scanning electron microscopy (SEM, HITACHI, S-3500N). Transmission electron microscopy (TEM) was performed on a JEM-2100 instrument. A dilute ethanol suspension of as-prepared samples was prepared via an ultrasonic dispersion and dropped onto a copper grid covered with a carbon film to make a specimen for TEM. N₂ adsorption data was measured using a NOVA 2000e (Quantachrome) instrument, and the specific surface area was evaluated by the BET method. UV-vis absorption spectra were recorded on a UV 2450 spectrophotometer.

2.2 Photoelectrical performance

The as-prepared materials were mixed with ethanol and stirred to obtain a fluid suspension. A film was made by the doctor blade method on fluorine-doped tin oxide (FTO) conductive glass (LOF, TEC-15, 15 Ω/square). After calcination in air for 30 minutes at 500 °C, the films were soaked in an ethanol based solution of N-719 dye for about 3 h. The dye-adsorbed ZnO electrode was assembled using clamps into a sandwich-type cell with a counter electrode (platinum sputtered FTO glass). A drop of electrolyte solution (0.5 M LiI + 0.05 M I₂ and 0.5 M 4-tert-butylpyridine in acetonitrile) was introduced into the clamped electrodes. The active electrode area employed was approximately 0.25 cm². Photocurrent-voltage (I-V) curves were measured at a Zahner CIMPS-2 electrochemical workstation using a Trusttech CHF-XM-500W source under simulated Sun

illumination (Global AM 1.5, 100 mW/cm²). Electrochemical impedance spectra (EIS) were collected using a Zahner CIMPS-2 electrochemical workstation. A perturbation of 10 mV was applied and data were collected from 100 kHz to 0.1 Hz. Intensity-modulated photovoltage spectroscopy (IMVS) and intensity-modulated photocurrent spectroscopy (IMPS) were carried out using a Zahner CIMPS-2 system. The lamp-house was fitted with a blue light emitting diode (LED) (470 nm) driven by a PP210 (Zahner) frequency response analyser. The LED provided both the dc and ac components of the illumination. The ac component of the current to the LED generated a modulation (10%) superimposed on the dc light intensity with a frequency range from 1000 Hz to 0.01 Hz for IMPS and IMVS.

2.3 UV-vis performance

The UV-vis absorbance and reflectance spectra were measured using a Shimadzu UV-2450 spectrophotometer. The ZnO films were calcined in air for 30 minutes at 500 °C. Then the films together with the FTO was used to measure the UV absorption and reflectance. To test the UV absorption and reflectance with dye N-719, the films (calcined) were soaked in an ethanol-based solution of N-719 dye for 3 h before testing.

3. Results and discussion

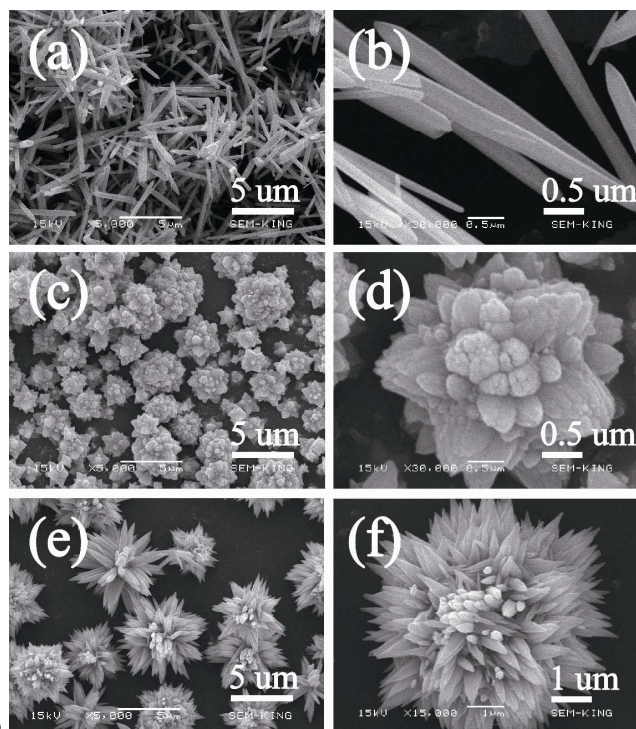


Fig. 1 SEM images of ZnO needles ((a), (b)), ZnO flowers ((c), (d)) and hedgehog-like ZnO needle-clusters ((e), (f)) obtained after calcination at 500 °C.

The morphology of the ZnO samples prepared can be clearly seen in the SEM images obtained which show 1-D needles, 3-D hierarchical flowers and 3-D hedgehog-like needle-clusters. As shown in Fig. 1a and 1b, the polyagonal structure can be clearly observed from the prismatic shape of the needles. The needles

show a diameter of around 0.2-0.4 μm and a length of 4-5 μm . It is obviously illustrated in Fig. 1c and Fig. 1d that the ZnO flowers are formed by the accumulation of several triangular shaped ‘petals’. The petals have sharp tips with wide bases which are connected to each other in flower-like morphologies, with the base of each petal connected at the centre of the flower. The typical diameter of a single flower is around 2-5 μm . The hedgehog-like hierarchical ZnO needle-clusters (Fig. 1e and Fig. 1f) are similar to the flowers, in which each individual ZnO needle-cluster is composed of well-aligned bundles of needles with spines originating from a single point. It should be noted that the diameter of a ZnO needle-cluster is about 4-6 μm , which is larger than the diameter of a flower. In theory, a larger crystalline grain is helpful for rapid transport of electrons.¹⁵ The varieties of ZnO nano/micromorphologies can be influenced by the synthesis process, alkaline concentration and selective adsorption of additives. In terms of needles and flowers, the stirring processes is largely responsible for the morphology evolution of ZnO. During the stirring process, ZnO particles form first. Then small particles through nucleation, followed by crystal growth to form larger needles. With a shorter stirring time, ZnO particles tend to generate and accumulate faster. Then these particles will agglomerate together to form flowers. In terms of hedgehog-like ZnO needle-clusters, low concentration of alkali accelerates the formation and growth of ZnO needles.

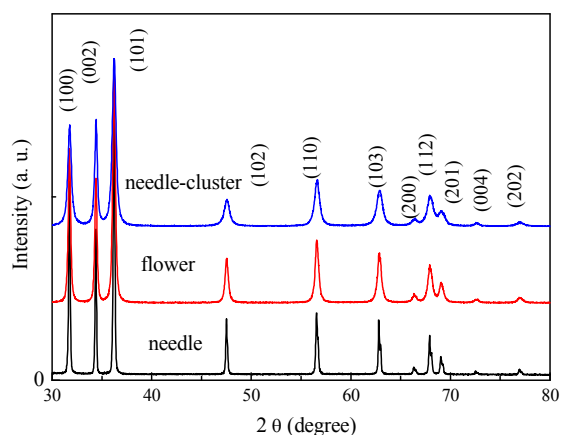


Fig. 2 XRD patterns of different ZnO nanomaterials.

The XRD patterns of the as-prepared samples are shown in Fig. 2 to demonstrate the crystallographic structures. As shown, all the diffraction peaks of the samples can be indexed to the hexagonal wurtzite structure of ZnO (PDF NO.36-1451) with unit cell constants of $a=3.252 \text{ \AA}$ and $c=5.213 \text{ \AA}$. No characteristic peaks of other impurities were detected in the patterns, suggesting that only single-phase ZnO was formed. Additionally, the strong peak intensities indicate a high quality of crystallization. Using the obtained XRD data, we obtain the lattice parameters for ZnO needles as $a = 3.2538$ and $c = 5.2098$, ZnO flowers as $a = 3.2543$ and $c = 5.2088$, hedgehog-like ZnO needle-clusters as $a = 3.2528$ and $c = 5.2063$.

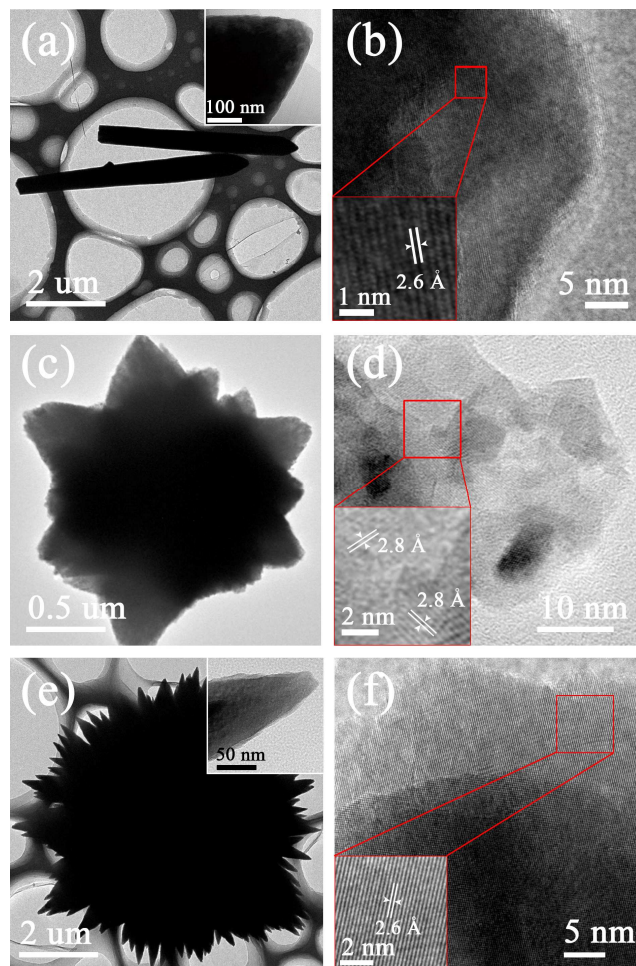


Fig. 3 TEM micrographs of ZnO needles (a, b), ZnO-flowers (c, d) and hedgehog-like hierarchical ZnO needle-clusters (e, f).

Transmission electron microscopy (TEM) observations give further insight into crystalline structure of the prepared ZnO samples (Fig. 3). As shown in Fig. 3a, the tops of the ZnO needles display a prism shape, which is attributed to the fast growth along the c axis direction. The crystal lattice fringes are clearly detected and the average distance between adjacent lattice planes is 2.6 \AA , which corresponds to the interplanar spacing of the (001) crystal planes in wurtzite ZnO. The corresponding SAED pattern (Figure S1a) of the ZnO needle can be indexed to the wurtzite structure of hexagonal ZnO and indicates its single-crystalline nature and its growth direction along [0001]. As seen from high resolution TEM (HRTEM), the ‘petals’ of the ZnO flowers are accumulated by randomly oriented ZnO nanoparticles, which act as rudiment of hexagonal structure. The lattice spacing is 2.8 \AA corresponding to the interplanar spacing of the (100) crystal planes of hexagonal ZnO (Fig. 3d). The corresponding SAED pattern (Figure S1b) corroborate the existence of the congregate ZnO nanoparticles. The hedgehog-like ZnO needle-clusters are formed with $\text{Zn}(\text{OH})_4^{2-}$ accumulated on the (001) positive surface of ZnO. Each ZnO needle is a single crystal which grows preferentially along a c -axis, and the needles grow from a common junction point which is beneficial for the electron

transport. The fringe spacing measured from a HRTEM image of an individual needle is 2.6 Å, which corresponds well to the interplanar spacing of the (001) crystal planes in wurtzite ZnO. Select-area electron diffraction (SAED) (Figure S1c) further confirms the each ZnO needle is preferentially oriented in the c axis direction with the single-crystal wurtzite structure.

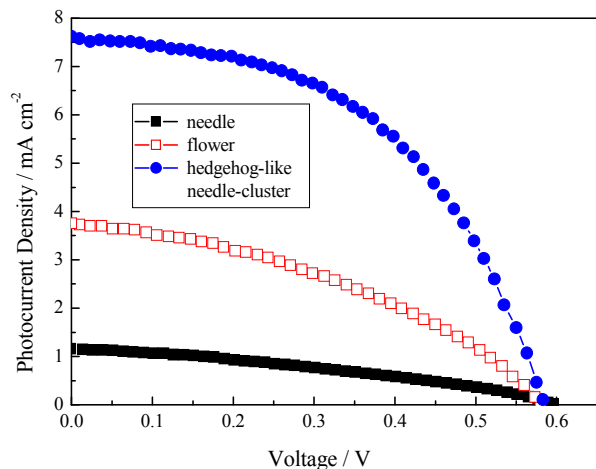


Fig. 4 I - V curves for DSSCs using different ZnO nanomaterials. Illumination intensity of 100 mW/cm² with Global AM 1.5 and an active area of 0.25 cm² are applied.

Table 1 Detailed photovoltaic parameters of DSSCs made of different ZnO nanomaterials calcined at 500 °C.

Sample	J_{sc} (mA/cm ²)	V_{oc} (V)	FF	η (%)	S_{BET} (m ² /g)
needle	1.16	0.596	0.34	0.24	10
flower	3.76	0.58	0.39	0.85	21
hedgehog-like needle-cluster	7.62	0.583	0.50	2.22	25

Fig. 4 shows the I - V curves of the corresponding DSSCs and Table 1 summarizes the measured and calculated values obtained. The short circuit current density (J_{sc}) and open circuit voltage (V_{oc}) of the ZnO needle DSSCs are 1.16 mA/cm² and 0.596 V, respectively. The conversion efficiency is only about 0.24 %. Compared to the needle DSSC, J_{sc} of the ZnO flower and hedgehog-like ZnO needle-cluster DSSCs are increased significantly, at 3.76 mA/cm² and 7.62 mA/cm², respectively. V_{oc} of the three DSSCs are almost identical. The conversion efficiency of the ZnO flower DSSC is about 0.85%, while a 2.22% efficiency is obtained for the hedgehog-like ZnO needle-cluster DSSC, which is about 3 times higher than the ZnO flower DSSC and 10 times higher than the ZnO needle DSSC. According to the BET results in Table 1, the specific surface areas of the ZnO flowers (21 m²/g) and hedgehog-like ZnO needle-clusters (25 m²/g) are larger than that of the ZnO needles (10 m²/g). The increased surface area would help adsorb more dye molecules to increase the light harvesting ability. The hedgehog-like ZnO needle-cluster DSSC shows a better fill factor (FF) (50 %) than that of the ZnO needle DSSC (34%), which may be attributed to the reduced recombination of charges at the interface between the hedgehog-like ZnO needle-cluster and I⁻/I₃⁻ electrolyte.⁵⁰

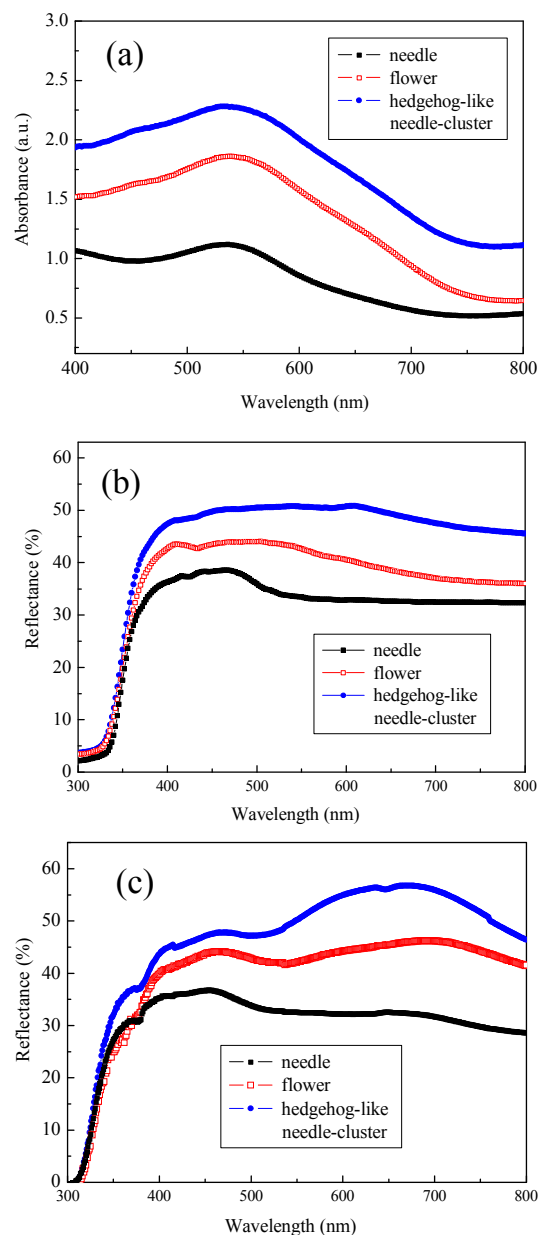


Fig. 5 (a) Optical absorption spectra of N-719 dye-sensitized ZnO electrodes; (b) UV-vis diffused reflectance spectra of different ZnO nanomaterials; (c) the UV reflectance spectra of ZnO nanomaterials after dye adsorption.

Fig. 5a shows the optical absorption spectra of N-719 dye-sensitized ZnO electrodes. The observed peak around 535 nm corresponds to the absorption of dye N-719. Dye adsorbed on hedgehog-like ZnO needle-clusters and ZnO flowers show higher absorption than ZnO needles, which indicate adsorbing a relatively larger amount of N-719. This is in agreement with the BET and the I - V results. Higher light scattering ability is another way to improve the light harvesting efficiency. The UV-vis reflectance spectra of the samples are given in Fig. 5b. Obviously, the reflectance spectrum of the hedgehog-like ZnO needle-clusters is higher than that of ZnO flowers and ZnO needles, indicating the hedgehog-like ZnO needle-clusters have a higher

light scattering ability than the other two structures. Taking account into the close relationship between morphology and light scattering, it could be attributed to the unique morphology.⁵¹⁻⁵² The hedgehog-like ZnO needle-clusters could effectively enhance the optical path length by multiple scattering and may lead to a photon localization effect that comes from confined light scattering. Therefore, more incident photons could be captured for useful transport.⁵²⁻⁵³ Higher light scattering could maximize the use of solar light thus improving the light harvesting efficiency^{45, 54-55} which would increase the short current density to some extent. Generally, both the higher dye loading and light scattering ability of the hedgehog-like ZnO needle-cluster contributes to the higher photocurrent density and power conversion efficiency. After dye adsorption, the reflectance of the ZnO film decreases drastically in the short wavelength ranging from 360 to 600 nm (Fig. 6c), which is mainly attributed to light absorption by the dye molecules. In the long wavelength region, the dye-adsorbed hedgehog-like ZnO needle-clusters film still remained a substantially higher reflectance than the dye-adsorbed ZnO needles, which suggests a higher short current density.

Fig. 6 shows the electrochemical impedance spectra (EIS) of the three different DSSCs. As is shown, there are two semicircles on the EIS plots, of which the one in the low frequency region shows a bigger radius than the other one in the higher frequency region. The large semicircles in the lower frequency region are assigned to the charge-transfer process occurring at the ZnO/dye/electrolyte interface (R_{ct}) and the small semicircles in the higher frequency region correspond to the resistance of the Pt/redox (I/I_3^-) interface charge transfer (R_{pt}).^{28,56-57} The R_{pt} values of the three different structures are very close, and are much smaller compared to the corresponding R_{ct} values. The charge-transfer resistance at the ZnO/dye/electrolyte interface (R_{ct}) for the three DSSCs is clearly different, showing the order: ZnO needle > ZnO flower > hedgehog-like ZnO needle-cluster. This means the charge transfer processes have a different rate: ZnO needle < ZnO flower < hedgehog-like ZnO needle-cluster.

This order is in agreement with the photoelectrochemical performance for the corresponding DSSCs. Furthermore, the fitting results based on the equivalent circuit (Fig. 6, inset)⁵⁸ are summarized in Table 2. Generally, the three ZnO structures have a similar Pt/redox (I/I_3^-) interface charge transfer resistance, of

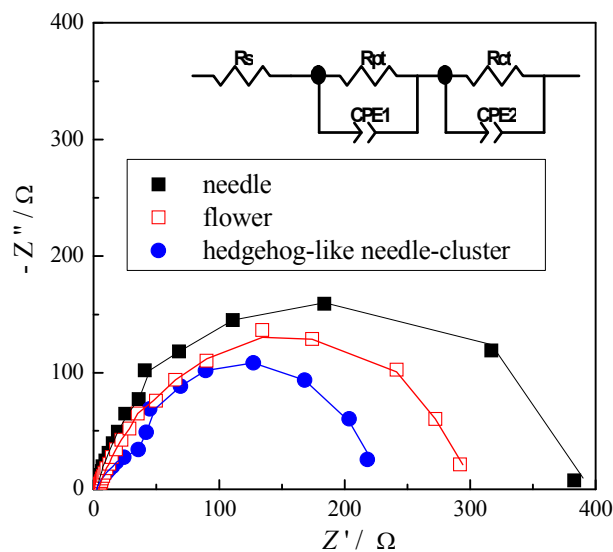


Fig. 6 Nyquist plots of the DSSCs made of different ZnO nanomaterials. The inset shows the equivalent circuit for the impedance spectrum. R_s : serial resistance; R_{pt} : charge-transfer resistance of Pt electrode; R_{ct} : charge-transfer resistance of photoanode; CPE: a constant phase element.

around 40 Ω . However, the charge-transfer resistance of hedgehog-like ZnO needle-clusters is much lower than that of ZnO needles and ZnO flowers. This can be attributed to not only the relative high surface area, but also to the fact that the liquid electrolyte can easily interpenetrate the structure of the hedgehog-like ZnO needle-clusters compared to the ZnO needles. In general, the hedgehog-like ZnO needle-clusters used as photoanode materials can provide a lower charge-transfer resistance than the other two structures. This could be an important factor for the improvement of the photoelectrochemical performance.

IMPS and IMVS were used to further investigate the electron transport and recombination processes as shown in Fig. 7. The electron transport time (τ_d) and the recombination time (τ_n , also electron lifetime) can be estimated from the IMPS and IMVS plots,^{28,59-62} respectively. As listed in Table 2, the electron transport time (τ_d) in ZnO flowers is longer than those in ZnO needles and hedgehog-like ZnO needle-clusters, which results from much grain interfaces existing in ZnO flowers. However, the ZnO needles and hedgehog-like ZnO needle-clusters are single crystals and oriented along the c axis direction which shows fewer defects, providing a direct and effective conduction

Table 2 Fitted data from EIS spectra and detailed IMPS/IMVS parameters for DSSCs made of different ZnO nanomaterials calcined at 500 °C.

	R_{pt} (Ω)	R_{ct} (Ω)	τ_d (ms)	τ_n (ms)	D_n (cm^2/s)	L_n (μm)
needle	39	347	4.62	179	2.16×10^{-4}	62.3
flower	39	255	6.4	354	1.56×10^{-4}	74.4
hedgehog-like needle-cluster	40	169	4.62	740	2.16×10^{-4}	126.6

pathway for rapid electron transport. The electron lifetime corresponding to hedgehog-like ZnO needle-clusters is obviously longer than ZnO needles and ZnO flowers. A longer electron lifetime indicates that a lower recombination possibility in hedgehog-like hierarchical ZnO needle-clusters, which is beneficial for high performance DSSCs. As reported previously, the interface recombination loss in ZnO-based DSSCs is mostly due to the uncovered oxide surface without dye molecules anchored.⁵⁵ Once the oxide makes contact with the electrolyte, the probability of charge recombination between electrons in the oxide and holes in the electrolyte will increase. For ZnO needles, the gaps (pores) located in the bottom of the film will be very small and the molecular dye will not easily reach into some of these regions, leading to inefficient dye loading and increasing the probability of surface recombination. Additionally, the accumulation of Zn²⁺/dye aggregate in the small pores will increase recombination.⁶³⁻⁶⁴ However, the conditions with hedgehog-like ZnO needle-clusters are very different. This special formation produces more large gaps for dye reaching, so the recombination in this case would be effectively suppressed.

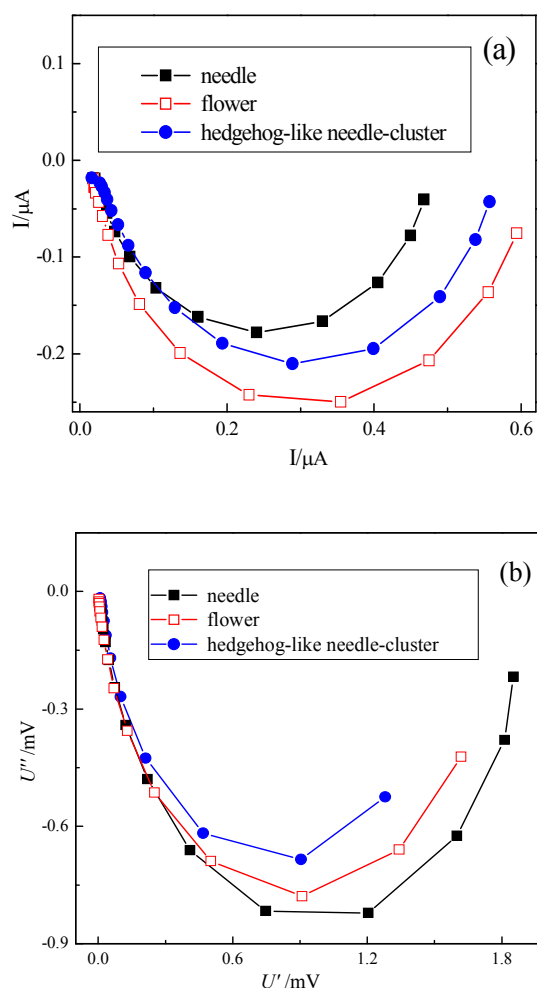


Fig. 7. Short-circuit IMPS response (a) and IMVS response (b) of dye-sensitized cells with different ZnO nanomaterials.

The electron diffusion coefficient can be estimated from the relation:

$$D_n \approx \frac{d^2}{\tau_d} \quad (1)$$

where d is the layer thickness of the ZnO structure and τ_d is the electron transport time. The electron diffusion length can be calculated from the layer thickness, electron transport time and electron lifetime:⁶⁵⁻⁶⁶

$$L = \sqrt{\frac{\tau_n}{\tau_d}} \quad (2)$$

The calculated results are listed in Table 3. The condition and number of boundaries among the ZnO structures and the surfaces influence the diffusion coefficient. ZnO flowers composed of nanoparticles show more boundaries than ZnO needles and hedgehog-like ZnO needle-clusters, which indicate a lower electron diffusion coefficient. The electron diffusion length demonstrates the competition between the electron back-reaction and the collection of electrons by diffusion to the substrate contact, which is an important factor for DSSCs. To efficiently collect photogenerated electrons at the back-contact, L_n should be greater than the film thickness. As shown in Table 3, the L_n values of the three ZnO structures are well above the film thickness of 10 μm , indicating high efficiencies as most photogenerated electrons are collected at the back contact, especially for the hedgehog-like hierarchical ZnO needle-clusters in which L_n value can reach up to 126.6 μm .

As described above, the hedgehog-like ZnO needle-clusters used in DSSCs provide not only low charge-transfer resistance but also long electron lifetimes, and benefits from the structural features of the one-dimensional ZnO with hedgehog-like hierarchical structures. A proposed model of electron transfer in the hedgehog-like ZnO needle-clusters is shown in Fig. 8. The electrons injected into the ZnO needles are transferred along the one-dimensional axis, and then collected at the bottom of the hedgehog-like hierarchical ZnO needle-clusters, from which they could rapidly transported to the FTO substrate or another hedgehog-like ZnO needle-clusters. Obviously, the resistance of the ZnO needle-clusters is reduced greatly due to the small grain size and high surface area, compared to ZnO needles and ZnO flowers as shown in Fig. 6, which could also indicate that the electron transport time and electron lifetime are similar to those for the needles as shown in Fig. 5. The single crystal and c axis oriented hedgehog-like ZnO needle-clusters show less defects which could provide a direct and effective conduction pathway for rapid electron transport, the same as ZnO needles. Moreover, the special structure of hedgehog-like ZnO needle-clusters produces more large gaps for dye reaching, and further effectively suppresses recombination compared to ZnO needles. Therefore, the hedgehog-like hierarchical ZnO needle-clusters show superior electron transfer kinetics: fast electron transfer and long life times with suppressed recombination.

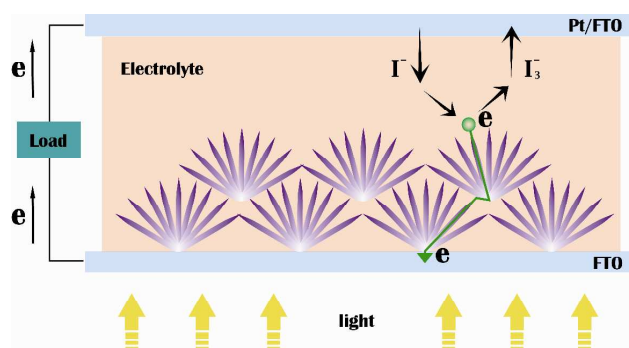


Fig. 8. Schematic diagram of the dye-sensitized solar cell with hedgehog-like hierarchical ZnO needle-clusters as the photoanode on FTO, showing the processes involved in current generation.

Conclusions

In conclusion, three forms of ZnO nanomaterials have been successfully synthesized by an optimized facile hydrothermal method, of these the hedgehog-like hierarchical ZnO needle-clusters show superior photoelectrochemical properties compared to the other two. The photovoltaic conversion efficiency of the ZnO needle-cluster DSSCs can reach up to 2.2% which is 10 times higher than the ZnO needle DSSCs. The good photoelectrochemical properties are attributed to strong light scattering, diffuse reflection and high surface area to enhance light harvesting. Additionally, the electrolyte can easily infiltrate into ZnO needle-clusters to reduce charge transfer resistance. The ZnO needle-cluster shows superior electron transfer kinetics: fast electron transfer and long lifetimes with suppressed recombination. This result is important for the design of efficient photoanode materials with optimum structures for DSSCs.

Acknowledgements

Kai Xi wishes to thank the Cambridge Overseas Trust. This work has been supported by the National Natural Science Foundation of China (21301022) and the Natural Science Foundation (no. 12KJB430001) of Jiangsu Education Committee of China. The authors would like to thank Nina Klein and Yanjun Liu for their assistance in preparing the paper for publication.

Notes and references

^a Center for low-dimensional materials, micro-nano devices and system, Changzhou University, Changzhou 213164, China Jiangsu Key Laboratory for Solar Cell Materials and Technology, Changzhou, 213164, China. Email: dingjn@cczu.edu.cn

^b Department of Materials Science and Metallurgy, University of Cambridge, Cambridge, CB2 3QZ, UK. Email: kx210@cam.ac.uk

^c China National Academy of Nanotechnology & Engineering, Teda, Tianjin, 300457, China.

^d Department of Chemistry and Geochemistry, Colorado School of Mines, 1500 Illinois Street, Golden, CO 80401.

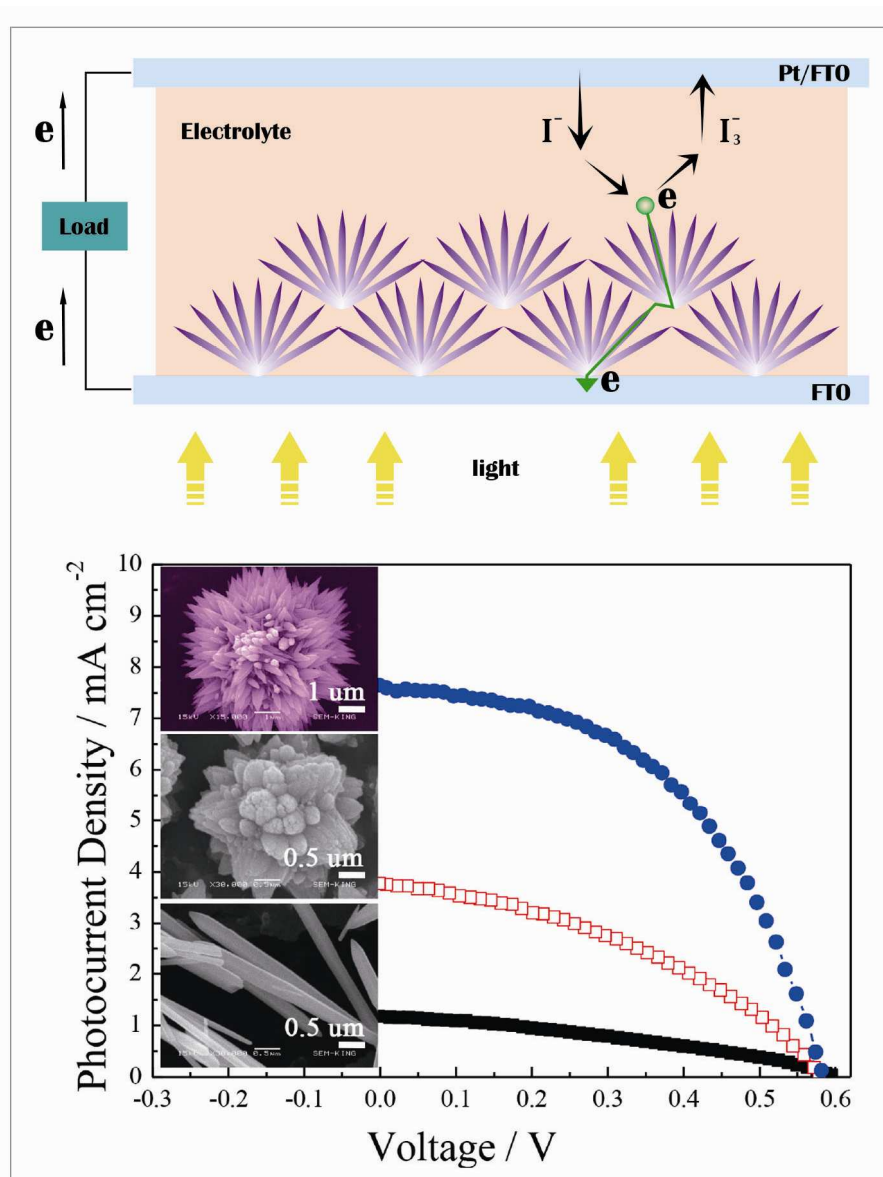
† Electronic Supplementary Information (ESI) available: [details of any supplementary information available should be included here]. See DOI: 10.1039/b000000x/

‡ Footnotes should appear here. These might include comments relevant to but not central to the matter under discussion, limited experimental and spectral data, and crystallographic data.

1 M. Grätzel, *J. Photochem. Photobiol. A.*, 2004, **164**, 3.

- 2 M. K. Nazeeruddin, P. Pechy, T. Renouard, S.M. Zakeeruddin, R. Humphry-Baker, P. Comte, P. Liska, L. Cevey, E. Costa, V. Shklover, L. Spiccia, G.B. Deacon, C.A. Bignozzi and M. Grätzel, *J. Am. Chem. Soc.*, 2001, **123**, 1613.
- 3 M. Pagliaro, G. Palmisano, R. Ciriminna and V. Loddo, *Energy Environ. Sci.*, 2009, **2**, 838.
- 4 G. R. Li, F. Wang, Q. W. Jiang, X. P. Gao and P. W. Shen, *Angew. Chem. Int. Ed.*, 2010, **49**, 3653.
- 5 G. R. Li, J. Song, G. L. Pan and X. P. Gao, *Energy Environ. Sci.*, 2011, **4**, 1680.
- 6 L. Wang, Z. S. Xue, X. Z. Liu and B. Liu, *RSC Adv.*, 2012, **2**, 7656.
- 7 A. A. Madhavan, S. Kalluri, D. K. Chacko, T. A. Arun, S. Nagarajan, K. R. V. Subramanian, A. S. Nair, S. V. Nair and A. Balakrishnan, *RSC Adv.*, 2012, **2**, 13032.
- 8 M. Grätzel, *Nature*, 2001, **414**, 338.
- 9 S. A. Haque, E. Palomares, B. M. Cho, A. N. M. Green, N. Hirata, D. R. Klug and J. R. Durrant, *J. Am. Chem. Soc.*, 2005, **127**, 3456.
- 10 K. Pan, Y. Z. Dong, C. G. Tian, W. Zhou, G. H. Tian, B. F. Zhao and H. G. Fu, *Electrochim. Acta*, 2009, **54**, 7350.
- 11 T. Berger, T. Lana-Villarreal, D. Monllor-Satoca and R. Gomez, *J. Phys. Chem. C.*, 2007, **111**, 9936.
- 12 D. H. Chen, F. Z. Huang, Y. B. Cheng and R. A. Caruso, *Adv. Mater.*, 2009, **21**, 1.
- 13 J. F. Qian, P. Liu, Y. Xiao, Y. Jiang, Y. L. Cao, X. P. Ai and H. X. Yang, *Adv. Mater.*, 2009, **21**, 3633.
- 14 M. J. Bierman and S. Jin, *Energy Environ. Sci.*, 2009, **2**, 1050.
- 15 J. Qu, G. R. Li, and X. P. Gao, *Energy Environ. Sci.*, 2010, **3**, 2003.
- 16 F. Zhu, D. P. Wu, Q. Li, H. Dong, J. M. Li, K. Jiang and D. S. Xu, *RSC Adv.*, 2012, **2**, 11629.
- 17 Z. H. Liu, X. J. Su, G. L. Hou, S. Bi, Z. Xiao and H. P. Jia, *RSC Adv.*, 2013, **3**, 8474.
- 18 H. Yu, B. F. Xue, P. Liu, J. X. Qiu, W. Wen, S. Q. Zhang, H. J. Zhao, *ACS Appl. Mater. Interfaces*, 2012, **4**(3), 1289.
- 19 P. N. Zhu, Y. Z. Wu, M. V. Reddy, A. S. Nair, S. J. Peng, N. Sharma, V. K. Peterson, B. V. R. Chowdari and S. Ramakrishnan, *RSC Adv.*, 2012, **2**, 5123.
- 20 J. R. Huang, X. Tan, T. Yu, L. Zhao and S. Xue, *RSC Adv.*, 2012, **2**, 12657.
- 21 S. H. Lim and S. W. Rhee, *RSC Adv.*, 2011, **1**, 518.
- 22 H. M. Zhang, H. Yu, Y. H. Han, P. Liu, S. Q. Zhang, P. Wang, Y. B. Cheng, H. J. Zhao, *Nano Res.*, 2011, **4**(10), 938.
- 23 A. Yella, H. W. Lee, H. N. Taso, C. Y. Yi, A. K. Chandiran, M. K. Nazeeruddin, E. W. G. Diau, C. Y. Yeh, S. M. Zakeeruddin and M. Grätzel, *Science*, 2011, **334**, 629.
- 24 X. Y. Wang, L. D. Sun, S. Zhang, X. Wang, K. F. Huo, J. J. Fu, H. R. Wang and D. L. Zhao, *RSC Adv.*, 2013, **3**, 11001.
- 25 S. Sadhuab and P. Poddar, *RSC Adv.*, 2013, **3**, 10363.
- 26 X. L. Liu, J. Lin and X. F. Chen, *RSC Adv.*, 2013, **3**, 4885.
- 27 Z. B. Tian, L. Q. Wang, L. S. Jia, Q. B. Li, Q. Q. Song, S. Su and H. Yang, *RSC Adv.*, 2013, **3**, 6369.
- 28 J. Qu, X. P. Gao, G. R. Li, Q. W. Jiang and T. Y. Yan, *J. Phys. Chem. C*, 2009, **113**, 3359.
- 29 S. A. Patil, D. V. Shinde, E. Kim, J. K. Lee, R. S. Mane and S. H. Han, *RSC Adv.*, 2012, **2**, 11808.
- 30 J. Guan, J. Y. Zhang, T. Yu, G. G. Xue, X. R. Yu, Z. K. Tang, Y. L. Wei, J. Yang, Z. S. Li and Z. G. Zou, *RSC Adv.*, 2012, **2**, 7708.
- 31 J. Chen, C. Li, F. Xu, Y. D. Zhou, W. Lei, L. T. Sun and Y. Zhang, *RSC Adv.*, 2012, **2**, 7384.
- 32 H. D. Zheng, Y. Tachibana and K. Kalantar-Zadeh, *Langmuir*, 2010, **26**, 19148.
- 33 J. R. Jennings, L. M. Peter, *J. Phys. Chem. C.*, 2007, **111**, 16100.
- 34 C. X. He, B. X. Lei, Y. F. Wang, C. Y. Su, Y. P. Fang, D. B. Kuang, *Chem. Eur. J.*, 2010, **16**, 8757.
- 35 C. H. Ku, J. J. Wu, *Nanotechnology*, 2007, **18**, 505706.
- 36 M. Quintana, T. Edvinsson, A. Hagfeldt, G. Boschloo, *J. Phys. Chem. C.*, 2007, **111**, 1035.
- 37 A. Otsuka, K. Funabiki, N. Sugiyama, T. Yoshida, *Chem. Lett.*, 2006, **35**, 666.
- 38 V. Kumar, N. Singh, V. Kumar, L. P. Purohit, A. Kapoor, O. M. Ntwaeaborwa and H. C. Swart, *J. Appl. Phys.*, 2013, **114**, 134506.

- 39 V. Kumar, R. G. Singh, N. Singh, A. Kapoor, R. M. Mehra, L. P. Purohit, *Mater. Res. Bull.*, 2013, **48**, 362.
- 40 V. Kumar, H. C. Swart, O. M. Ntwaeaborwa, R. E. Kroon, J. J. Terblans, S. K. K. Shaat, A. Yousif, M. M. Duvenhage, *Mater. Lett.*, 2013, **101**, 57.
- 41 A. B. F. Martinson, J. W. Elam, J. T. Hupp, M. J. Pellin, *Nano Lett.*, 2007, **7**, 2183.
- 42 R. Zhang, S. Kumar, S. Zou and L. L. Kerr, *Cryst. Growth. Des.*, 2008, **8**, 381.
- 43 W. T. Sun, Y. Yu, H. Y. Pan, X. F. Gao, Q. Chen and L. M. Peng, *J. Am. Chem. Soc.*, 2008, **130**, 1124.
- 44 L. Y. Chen and Y. T. Yin, *RSC Adv.*, 2013, **3**, 8480.
- 45 S. B. Zhu, L. M. Shan, X. N. Chen, L. He, J. J. Chen, M. Jiang, X. L. Xie and Z. W. Zhou, *RSC Adv.*, 2013, **3**, 2910.
- 46 C. T. Wu, W. P. Liao and J. J. Wu, *J. Mater. Chem.*, 2011, **21**, 2871.
- 47 S. H. Kang, S. H. Choi, M. S. Kang, J. Y. Kim, H. S. Kim, T. Hyeon and Y. E. Sung, *Adv. Mater.*, 2008, **20**, 54.
- 48 K. Zhu, N. R. Neale, A. Miedaner and A. J. Frank, *Nano Lett.*, 2007, **7**, 69.
- 49 J. Jen Wu, G. R. Chen, H. H. Yang, C. H. Ku, and J. Y. Lai, *Appl. Phys. Lett.*, 2007, **90**, 213109.
- 50 C. Y. Jiang, X. W. Sun, G. Q. Lo, D. L. Kwong, and J. X. Wang, *Appl. Phys. Lett.*, 2007, **90**, 263501.
- 51 C. Lévy-Clément, J. Elias, R. Tena-Zaera, *Phys. Status Solidi C*, 2009, **7**, 1596.
- 52 C. Cheng, Y. Shi, C. Zhu, W. Li, L. Wang, K. K. Fung and N. Wang, *phys. Chem. Chem. Phys.*, 2011, **13**, 10631.
- 53 F. Xu and L. T. Sun, *Energy Environ. Sci.*, 2011, **4**, 818.
- 54 J. Y. Liao, B. X. Lei, D. B. Kuang and C. Y. Su, *Energy Environ. Sci.*, 2011, **4**, 4079.
- 55 J. Y. Liao, H. P. Lin, H. Y. Chen, D. B. Kuang and C. Y. Su, *J. Mater. Chem.*, 2011, **22**, 1627.
- 56 L. Y. Han, N. Koide, Y. Chiba and T. Mitate, *Appl. Phys. Lett.*, 2004, **84**, 2433.
- 57 M. Adachi, M. Sakamoto, J. T. Jiu, Y. Ogata and S. Isoda, *J. Phys. Chem. B*, 2006, **110**, 13872.
- 58 K. M. Lee, V. Suryanarayanan and K. C. Ho, *Sol. Energy Mater. Sol. Cells*, 2007, **91**, 1416.
- 59 M. Adachi, M. Sakamoto, J. T. Jiu, Y. Ogata and S. Isoda, *J. Phys. Chem. B*, 2006, **110**, 13872.
- 60 L. Bay and K. West, *Sol. Energy Mater. Sol. Cells*, 2005, **87**, 613.
- 61 D. S. Zhang, T. Yoshida, T. Oekermann, K. Furuta and H. Minoura, *Adv. Funct. Mater.*, 2006, **16**, 1228.
- 62 B. H. Lee, M. Y. Song, S. Y. Jang, S. M. Jo, S. Y. Kwak and D. Y. Kim, *J. Phys. Chem. C*, 2009, **113**, 21453.
- 63 K. Keis, E. Magnusson, H. Lindstrom, S. Lindquist, and A. Hagfeldt, *Sol. Energy Mater. Sol. Cells.*, 2002, **73**, 51.
- 64 K. Keis, J. Lindgren, S. E. Lindquist, and A. Hagfeldt, *Langmuir*, 2000, **16**, 4688.
- 65 G. Franco, J. Gehring, L. M. Peter, E. A. Ponomarev, I. Uhlendorf, *J. Phys. Chem. B.*, 1999, **103**, 692.
- 66 G. Franco, L. M. Peter, E. A. Ponomarev, *Electrochem. Commun.*, 1999, **1**, 61.



Owing to their unique morphology hedgehog-like ZnO needle-clusters show enhanced photovoltaic conversion efficiencies and superior electron transfer kinetics: fast electron transfer and long lifetimes with suppressed recombination.

SUPPORTING INFORMATION

Hedgehog-like hierarchical ZnO needle-clusters with superior electron transfer kinetics for dye-sensitized solar cells

Jie Qu,^a Yongan Yang,^d Qingduan Wu,^c Paul R. Coxon,^b Yingjun Liu,^b Xiong He,^b
Kai Xi,^{*b} Ningyi Yuan^a and Jianning Ding^{*a}

a Center for low-dimensional materials, micro-nano devices and system, Changzhou University, Changzhou 213164, China

Jiangsu Key Laboratory for Solar Cell Materials and Technology, Changzhou, 213164, China. Email: dingjn@cczu.edu.cn

b Department of Materials Science and Metallurgy, University of Cambridge, Cambridge, CB2 3QZ, UK. Email:

kx210@cam.ac.uk

c China National Academy of Nanotechnology & Engineering, Teda, Tianjin, 300457, China.

d Department of Chemistry and Geochemistry, Colorado School of Mines, 1500 Illinois Street, Golden, CO 80401

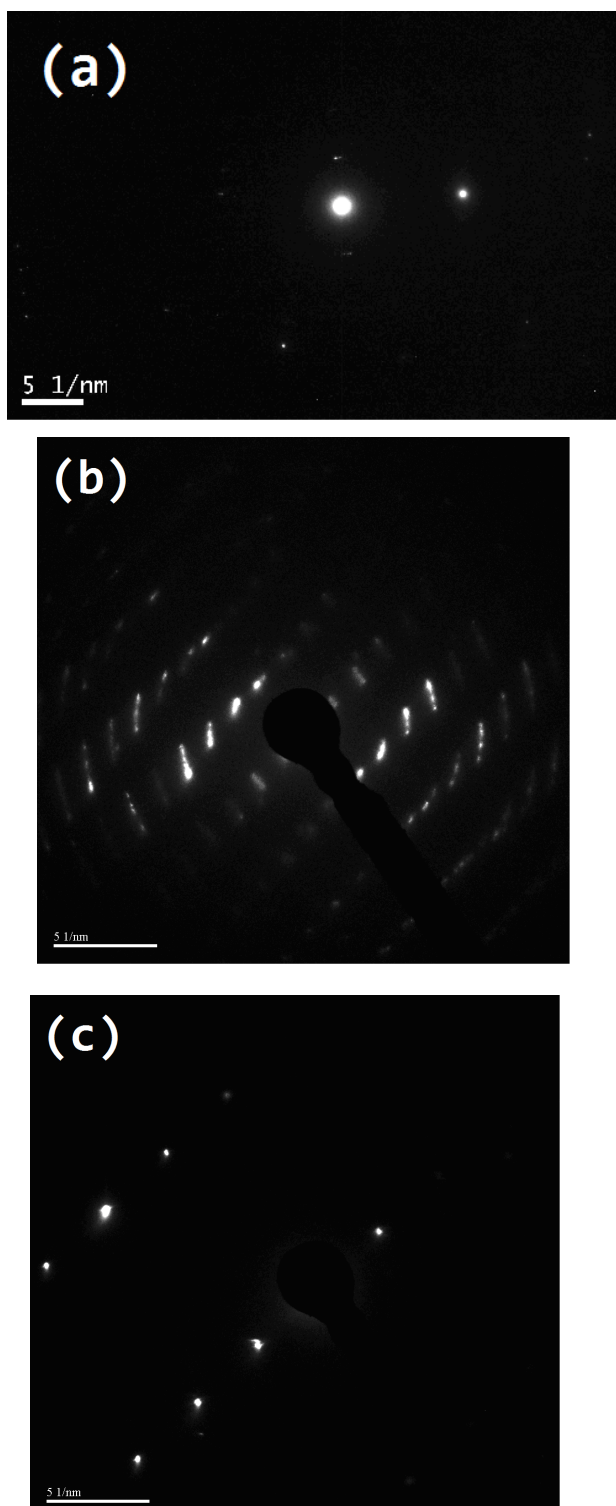


Fig. S1 SAED pattern of ZnO needles (a), ZnO-flowers (b) and hedgehog-like hierarchical ZnO needle-clusters (c).